

# In Situ Noise Characterization of the D-Wave Quantum Annealer

Tristan Zaborniak

Department of Physics and Astronomy  
University of Victoria  
Victoria, Canada  
tristanz@uvic.ca

Rogério de Sousa

Department of Physics and Astronomy  
University of Victoria  
Victoria, Canada  
rdesousa@uvic.ca

**Abstract**—Magnetic flux noise limits the performance of quantum computers based on superconducting flux qubits by altering their states in an uncontrolled manner throughout computations and reducing their coherence time. In quantum annealers, this noise introduces fluctuations to the linear constants of the original problem Hamiltonian, such that they find the ground states of problems perturbed from those programmed. Here we describe how to turn this drawback into a method to probe the flux noise frequency dependence *in situ* of the D-Wave 2000Q quantum annealer. The method relates the autocorrelation of the readout-state of a qubit repeatedly collapsed from uniform superposition to that of the flux noise impinging on the qubit. We show that this leads to an estimate for the noise spectral density affecting D-Wave qubits under normal operating conditions. The method is general and can be used to characterize noise in all architectures for quantum annealing.

**Index Terms**—noise, quantum annealing, flux noise, superconducting qubit hardware

## I. INTRODUCTION

Quantum annealers are non-universal quantum computers designed to solve optimization problems [1]–[3]. Because quantum annealing (QA) has less stringent requirements on qubit control than gate-based quantum computing, it permits an easier route for scaling up to a large number of qubits. The company D-Wave Systems Inc. currently offers access to its 2000-qubit quantum annealer on its cloud-based platform D-Wave Leap, and has announced a 5000-qubit device that will be available in the near future [4].

The D-Wave quantum annealer (hereafter annealer) is a lattice of superconducting quantum interference device (SQUID) flux qubits [5]. It realizes the following programmable quantum Hamiltonian:

$$\mathcal{H}_{\text{QA}} = -\frac{A(t)}{2} \sum_i \sigma_x^{(i)} + \frac{B(t)}{2} \left[ \sum_i h_i \sigma_z^{(i)} + \sum_{i>j} J_{ij} \sigma_z^{(i)} \sigma_z^{(j)} \right], \quad (1)$$

where  $\sigma_x^{(i)}$  and  $\sigma_z^{(i)}$  are  $x$  and  $z$  Pauli matrices acting on qubit  $i$ , satisfying  $\sigma_z^{(i)} |\pm 1\rangle = \pm |\pm 1\rangle$  (it is convenient to denote the two qubit states by  $\{|+1\rangle, |-1\rangle\}$ , instead of the usual  $\{|0\rangle, |1\rangle\}$ ). The parameter  $h_i$  is called the “bias” on qubit

$i$ , and  $J_{ij}$  is called the “coupling” between qubits  $i$  and  $j$ . The  $h_i$  and  $J_{ij}$  are the programmable input parameters that define the problem to be solved. Time dependent constants  $A(t)$  and  $B(t)$  determine the annealing schedule. At  $t = 0$ ,  $A(0) \gg B(0)$  so that the ground state of the  $n$ -qubit system is in the superposition of all computational basis states,  $|\psi_0(0)\rangle = (|+1\rangle + |-1\rangle) \otimes \dots \otimes (|+1\rangle + |-1\rangle) / \sqrt{2^n}$ . As time evolves, the device decreases  $A(t)$  and increases  $B(t)$ , so that at time  $t = t_a$  (the end of the anneal schedule) it satisfies  $A(t_a) \ll B(t_a)$ . Under certain circumstances approaching the satisfaction of the adiabatic theorem [3], the system remains in the ground state throughout the time evolution, and each qubit state in  $|\psi_0(t_a)\rangle$  can be read-out to determine the lowest energy solution of the Ising Hamiltonian:

$$\mathcal{H}_{\text{Ising}}(\mathbf{s}) = \sum_i h_i s_i + \sum_{i>j} J_{ij} s_i s_j, \quad (2)$$

where  $s_i = \pm 1$  are (classical) Ising spin variables. As it turns out, the problem for finding the vector  $\mathbf{s}$  that minimizes Eq. (2) belongs to the NP-Hard complexity class of classical computation, and maps with polynomial overhead to a number of important combinatorial problems including travelling salesman, exact cover, and 3-satisfiability [6], [7].

Similar to all architectures for quantum computing, QA hardware is sensitive to electromagnetic noise from its solid-state environment. In the case of the D-Wave annealer, the bias coefficients of the problem Hamiltonian at  $t_a$  end up as  $h_i + \phi_i(t_a)$  instead of  $h_i$ , with the noise amplitude  $\phi_i(t_a)$  expected to occur due to intrinsic flux noise in the SQUIDs forming qubit  $i$ , as well as sources stemming from adjacent qubits and control hardware [8]. A notable consequence of  $\phi_i(t_a) \neq 0$  is that the system ends up solving the “wrong problem” even when the QA finds the correct ground state [9]. We refer to this effect as “Hamiltonian noise”.

Here we show that the presence of Hamiltonian noise in the D-Wave annealer can be exploited for *in situ* characterization of the amplitude and frequency dependence of the electromagnetic noise affecting qubits, identifying its physical origin and suggesting a method for benchmarking noise in future devices.

This work was supported by the Natural Sciences and Engineering Research Council of Canada through its Undergraduate Student Research Award and Discovery programs (RGPIN-2020-04328).

## II. DEGENERATE QUANTUM ANNEALING AS A WITNESS FOR TIME-CORRELATED HAMILTONIAN NOISE

We now describe a series of annealing experiments using the D-Wave Leap interface with the DW\_2000Q\_6 quantum processing unit (QPU). Our method is to solve the *degenerate* Ising problem ( $h_i = J_{ij} = 0$ ) over the qubits of the annealer  $N$  times over in immediate, periodic succession. Each run yields a set of 2000 time series  $\beta_i(j) = \pm 1$ , denoting the state of qubit  $i = 1, \dots, 2000$  readout at time  $t_j = (j + 1)\Delta t$ , where  $j = 0, \dots, N - 1$ . Here  $\Delta t = t_d + t_a$ , where  $t_d = 295 \mu\text{s}$  is the time it takes for initialization and readout, and  $t_a$  is the annealing time set by the user.

The time correlation function for the solution-state of qubit

$i$  at time  $t_k = k\Delta t$  is computed from:

$$\langle \beta(t_k)\beta(0) \rangle_i = \frac{1}{N-k} \sum_{j=0}^{N-k-1} \beta_i(j+k)\beta_i(j). \quad (3)$$

Clear from this definition is that as  $k$  increases, fewer observations of  $\beta_i(j+k)\beta_i(j)$  are used in calculating  $\langle \beta(t_k)\beta(0) \rangle_i$ , with only one observation being used in the case that  $k = N - 1$ . In our calculations, we chose to consider  $k = 0, 1, 2, \dots, N/2$  such that the maximum and minimum numbers of observations used in computing  $\langle \beta(t_k)\beta(0) \rangle_i$  differ by only a factor of 2. With  $N = 1000$ , this means that we use a minimum of 500 observations in computing  $\langle \beta(t_k)\beta(0) \rangle_i$ . Figures 1(a) and 1(b) shows the measured solution-state time correlation function for qubits  $i = 1$  and  $i = 2000$ , both for annealing time  $t_a = 1 \mu\text{s}$  ( $\Delta t = 296 \mu\text{s}$ ).

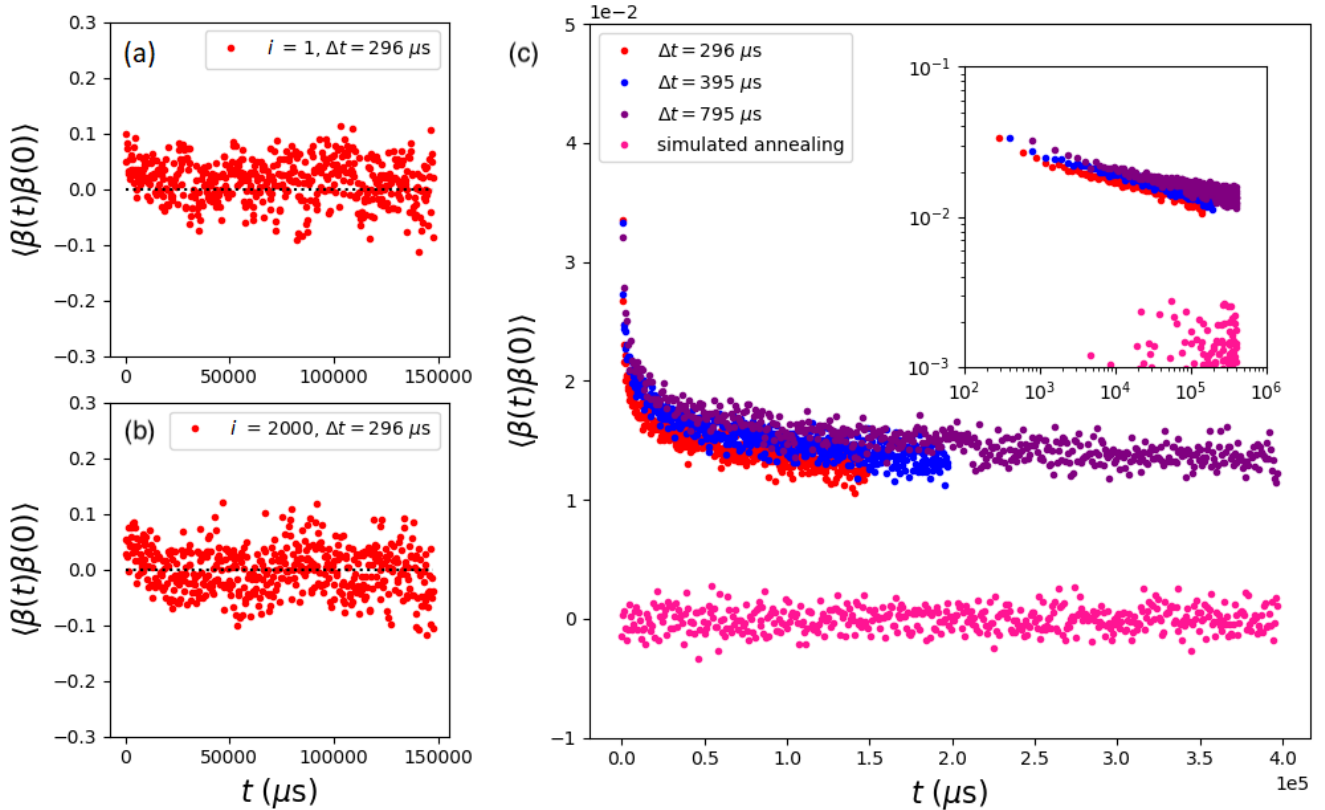


Fig. 1: Solution-state time correlation function obtained from  $N = 1000$  degenerate QA runs in the DW\_2000Q\_6 QPU. (a) Correlation function for qubit  $i = 1$ , for annealing time  $t_a = 1 \mu\text{s}$  ( $\Delta t = 296 \mu\text{s}$ ). (b) Same for qubit  $i = 2000$ . (c) Correlation functions after averaging over all 2000 qubits in lin-lin and log-log (inset), for  $t_a = 1, 100, 500 \mu\text{s}$ . For comparison we also show the correlation function obtained by sampling the same degenerate problem by classical simulated annealing using `neal` [4].

A significantly smoother version of the time correlation function is obtained by averaging over all 2000 qubits. Figure 1(c) shows this result for three different annealing times,  $t_a = 1, 100, 500 \mu\text{s}$ , corresponding to  $\Delta t = 296, 395, 795 \mu\text{s}$ . For comparison to what would be true in the absence of Hamiltonian noise, we also included the correlation function obtained by running the same degenerate problem by way of classical simulated annealing using `neal` (Fig. 1(c)). Clearly,

Fig. 1 reveals the presence of a long time tail in QA measurements. This is clear evidence for the presence of *colored noise* in the QPU, in contrast to the uncorrelated white noise of the simulator.

Our interpretation of this result is that the actual  $h_i$  parameters in the QPU differ from zero at readout. They are instead given by  $h_i = \phi_i(t_a)$  where  $\phi_i(t_a)$  is a stochastic process. In order to characterize the details of this process, we need

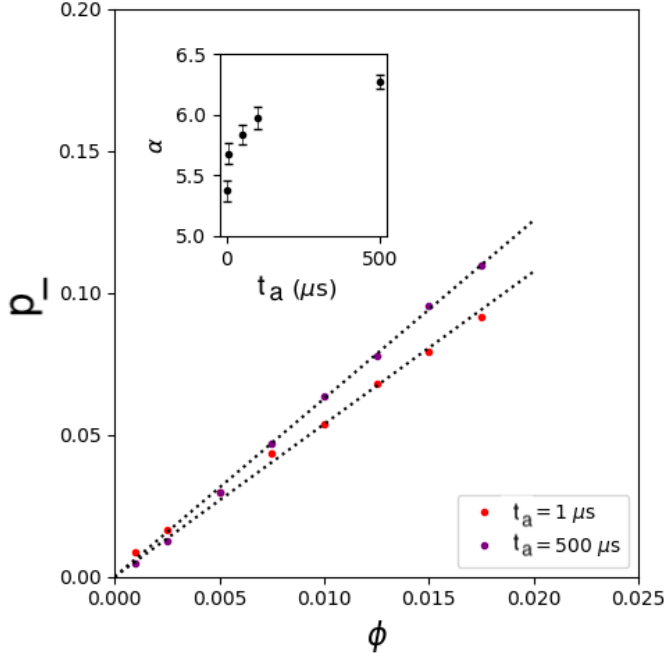


Fig. 2: Probability  $p_{-}$  for obtaining the one-qubit ground state  $|-\rangle$  for small values of  $h_i = \phi > 0$ . The linear relation  $p_{\pm} = \frac{1}{2} \mp \alpha(t_a)\phi$  holds with coefficient  $\alpha(t_a)$  depending on the annealing time  $t_a$  (inset).

to find the relationship between  $h_i$  and the probability for measuring the corresponding one-qubit ground state in the QA (e.g.  $p_{-} = p(|-1\rangle)$  for  $h_i > 0$ ) as a function of anneal time. To find  $p_{\pm}$  experimentally, we performed  $N = 1000$  “non-degenerate” QA runs for several small values of  $h_i = \phi > 0$ . We estimated  $p_{\pm}$  as the fraction of runs that the annealer measured  $+1$  or  $-1$  for the qubit state. The result is shown in Fig. 2 where we see that the linear relation:

$$p_{\pm} = \frac{1}{2} \mp \alpha(t_a)\phi \quad (4)$$

holds for  $\phi$  smaller than  $10^{-2}$ . Values for the coefficient  $\alpha(t_a)$  depend strongly on the annealing time  $t_a$ , as shown in the inset.

Armed with Eq. (4), we get an explicit relation between the correlation functions for  $\beta(t)$  and  $\phi(t)$ :

$$\begin{aligned} \langle \beta(t)\beta(0) \rangle &= \langle [p_{+}(t) - p_{-}(t)] [p_{+}(0) - p_{-}(0)] \rangle \\ &= 4\alpha^2(t_a)\langle \phi(t)\phi(0) \rangle. \end{aligned} \quad (5)$$

We should remark that this relation is based on the assumption that QA was used to probe  $\phi$ ; as a result, Eq. (5) requires  $t \geq \Delta t$ . It does not hold for  $t = 0$ , where  $\langle \beta(t)\beta(0) \rangle = 1$  by design, but  $\langle \phi(t)\phi(0) \rangle$  is not necessarily equal to  $1/[4\alpha^2(t_a)]$ .

Figure 3 shows the resulting  $\langle \phi(t)\phi(0) \rangle$  obtained using Eq. (5) with  $\alpha(t_a)$  adjusted within their ranges of uncertainty to yield a better collapse of the three different  $t_a$  curves.

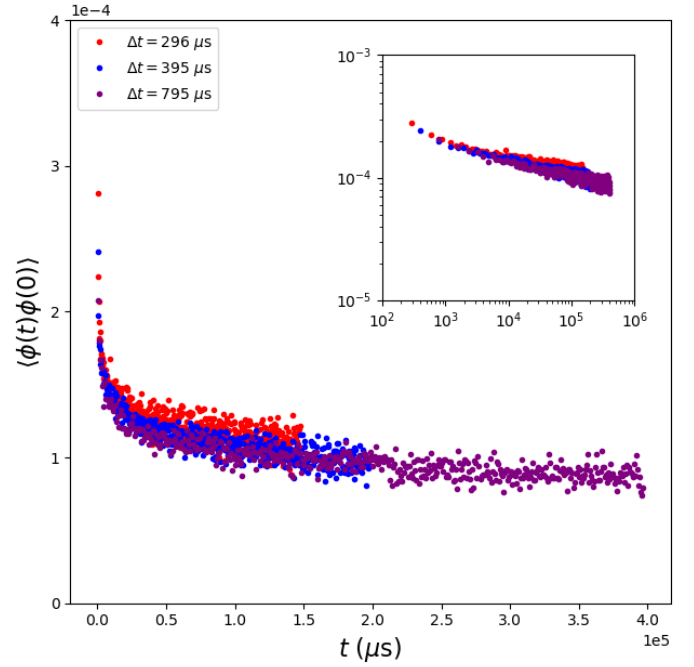


Fig. 3: Time correlation function for  $h_i = \phi$  averaged over all qubits, obtained from  $\langle \phi(t)\phi(0) \rangle = \langle \beta(t)\beta(0) \rangle / [4\alpha^2(t_a)]$ , see Eq. (5). Data shown for  $t_a = 1, 100, 500 \mu\text{s}$ . The log-log plot is shown in the inset.

### III. ESTIMATED POWER SPECTRAL DENSITY

We now obtain an estimate for the noise spectral density associated with  $\phi$ :

$$S_{\phi}(f) = \int_{-\infty}^{\infty} dt e^{2\pi i f t} \langle \phi(t)\phi(0) \rangle. \quad (6)$$

To do this, we applied the Welch method [10] directly to the  $\beta_i(t_j)$  time series, averaged over all qubits  $i$ , and divided by  $4\alpha^2(t_a)$  following Eq. (5). We used the largest possible segment length (`nperseg=N=1000`, the length of the time series [11]) to minimize the usual periodogram oscillations in the low frequency region. The result is shown in Fig. 4.

As pointed out above, the fact that  $\langle \beta^2 \rangle = 1$  gives an additional contribution to the correlation function  $\langle \phi(t)\phi(0) \rangle$  at  $t = 0$ . Because this contribution is present only at  $t = 0$ , it contributes an artifactual white noise background to  $S_{\phi}(f)$ . This white noise background enforces the satisfaction of the sum rule:

$$\int_0^{\frac{1}{2\Delta t}} df S_{\phi}(f) = \text{Lim}_{t \rightarrow 0} \langle \phi(t)\phi(0) \rangle = \frac{1}{4\alpha^2(t_a)}. \quad (7)$$

With Eq. (7) we are able to obtain a simple model that explains our measurements. We assume the noise is dominated by *universal magnetic flux noise* within the materials forming the SQUIDs [12]–[15] plus the artifactual white noise background:

$$S_{\phi}(f) = \left[ \left( \frac{A}{f} \right)^a + W \right] \mu\text{s}, \quad (8)$$

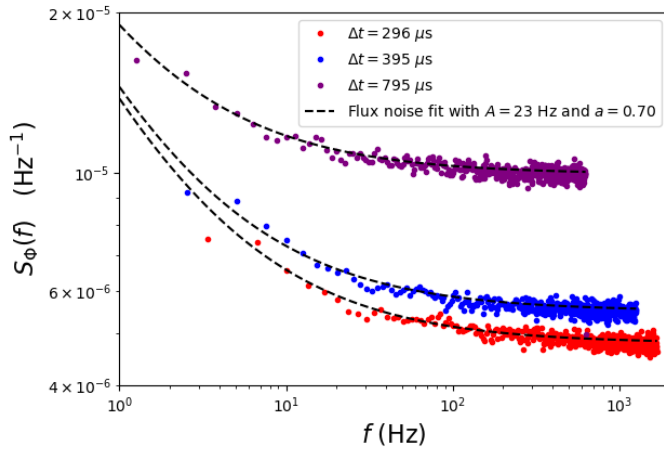


Fig. 4: Estimated noise spectral density using the Welch method. The dashed lines are universal fits based on Eq. (8) using two fitting parameters *independent* of  $\Delta t$ : The flux noise amplitude  $A = (23 \pm 1)$  Hz and the exponent  $a = (0.70 \pm 0.02)$ , plus the artifactual white noise background given by Eq. (9).

where the amplitude  $A$  and exponent  $a$  are fitting parameters independent of  $t_a$  and  $\Delta t$ . The white noise background  $W$  is calculated using Eq. (7) to be:

$$W = \frac{(\Delta t)}{2\alpha^2(t_a)\mu s} - \frac{[2(\Delta t)A]^a}{1-a}. \quad (9)$$

In order to fit the data we first removed the  $f = 0$  data points from the power spectral densities estimated with the Welch method, so that any static effect such as long-lived spin polarization [16] is subtracted from the data [note that Eq. (6) did not subtract  $\langle\phi(t)\rangle$  from the fluctuations of  $\phi$ ]. Equations (8) and (9) were used to fit all three curves simultaneously in Fig. 4 leading to  $A = (23 \pm 1)$  Hz and  $a = (0.70 \pm 0.02)$  (dashed lines) [17].

#### IV. CONCLUSIONS

In conclusion, we describe a method for *in situ* measurement of Hamiltonian noise in QA hardware, based on sampling the states of qubits after annealing the device in the degenerate regime. Applying this method to the D-Wave 2000Q device yields estimates for the qubit bias time correlation function  $\langle\phi(t)\phi(0)\rangle$  and its noise spectral density  $S_\phi(f)$ .

Our measurements of the time correlation function for the qubit bias  $\phi$  lead to an estimate for the uncertainty when programming bias  $h_i$  in QA. The rms uncertainty is  $\sqrt{\langle\phi^2\rangle} \approx \sqrt{\langle\phi(\Delta t)\phi(0)\rangle} = 2 \times 10^{-2}$  for  $\Delta t = 1 \mu s$ .

Moreover, the estimation of the noise spectral density  $S_\phi(f)$  for different annealing times  $t_a$  allows us to conclude that qubit bias noise is dominated by the  $1/f^{0.7}$  frequency dependence characteristic of universal flux noise *intrinsic to the materials* forming the device [12], [13], [15]. This shows that in the D-Wave annealer intrinsic noise currently plays a more important role than cross-talk due to adjacent qubits and control hardware.

#### ACKNOWLEDGMENT

We thank M. Amin, T. Lanting, A. Nava, and S. Tomkins for useful discussions and critical reading of the manuscript.

#### REFERENCES

- [1] M. W. Johnson, M. H. S. Amin, S. Gildert, T. Lanting, F. Hamze, N. Dickson, R. Harris, A. J. Berkley, J. Johansson, P. Bunyk, E. M. Chapple, C. Enderud, J. P. Hilton, K. Karimi, E. Ladizinsky, N. Ladizinsky, T. Oh, I. Perminov, C. Rich, M. C. Thom, E. Tolkacheva, C. J. S. Truncik, S. Uchaikin, J. Wang, B. Wilson, and G. Rose, "Quantum annealing with manufactured spins," *Nature*, vol. 473, p. 194, 2011.
- [2] S. Boixo, T. F. Rønnow, S. V. Isakov, Z. Wang, D. Wecker, D. A. Lidar, J. M. Martinis, and M. Troyer, "Evidence for quantum annealing with more than one hundred qubits," *Nat. Phys.*, vol. 10, p. 218, 2014.
- [3] T. Albash and D. A. Lidar, "Adiabatic Quantum Computation," *Rev. Mod. Phys.*, vol. 90, p. 15002, 2018.
- [4] "D-Wave Leap," <https://www.dwavesys.com/take-leap>, accessed: 2020-05-18.
- [5] R. Harris, J. Johansson, A. J. Berkley, M. W. Johnson, T. Lanting, S. Han, P. Bunyk, E. Ladizinsky, T. Oh, I. Perminov, E. Tolkacheva, S. Uchaikin, E. M. Chapple, C. Enderud, C. Rich, M. Thom, J. Wang, B. Wilson, and G. Rose, "Experimental demonstration of a robust and scalable flux qubit," *Phys. Rev. B*, vol. 81, p. 134510, 2010.
- [6] E. Farhi, J. Goldstone, S. Gutmann, J. Lapan, a. Lundgren, and D. Preda, "A quantum adiabatic evolution algorithm applied to random instances of an NP-complete problem." *Science*, vol. 292, p. 472, 2001.
- [7] A. Lucas, "Ising formulations of many np problems," *Frontiers in Physics*, vol. 2, p. 5, 2014.
- [8] "Technical Description of the D-Wave Quantum Processing Unit," [https://docs.dwavesys.com/docs/latest/doc\\_qpu.html](https://docs.dwavesys.com/docs/latest/doc_qpu.html), accessed: 2020-05-22.
- [9] A. Pearson, A. Mishra, I. Hen, and D. Lidar, "Analog Errors in Quantum Annealing: Doom and Hope," arXiv:1907.12678 [quant-ph]. [Online]. Available: <https://arxiv.org/abs/1907.12678>
- [10] P. D. Welch, "The use of fast fourier transform for the estimation of power spectra: A method based on time averaging over short, modified periodograms," *IEEE Transactions on Audio and Electroacoustics*, vol. 15, p. 70, 1967.
- [11] "See python function scipy.signal.welch," <https://docs.scipy.org/doc/scipy-0.14.0/reference/generated/scipy.signal.welch.html>, accessed: 2020-05-21.
- [12] F. C. Wellstood, C. Urbina, and J. Clarke, "Low frequency noise in dc superconducting quantum interference devices below 1 K," *Appl. Phys. Lett.*, vol. 50, p. 772, 1987.
- [13] T. Lanting, M. H. Amin, A. J. Berkley, C. Rich, S.-F. Chen, S. LaForest, and R. de Sousa, "Evidence for temperature-dependent spin diffusion as a mechanism of intrinsic flux noise in SQUIDS," *Phys. Rev. B*, vol. 89, p. 014503, 2014.
- [14] S. LaForest and R. de Sousa, "Flux-vector model of spin noise in superconducting circuits: Electron versus nuclear spins and role of phase transition," *Phys. Rev. B*, vol. 92, p. 054502, 2015.
- [15] C. M. Quintana, Y. Chen, D. Sank, A. G. Petukhov, T. C. White, D. Kafri, B. Chiaro, A. Megrant, R. Barends, B. Campbell, Z. Chen, A. Dunsforth, A. G. Fowler, R. Graff, E. Jeffrey, J. Kelly, E. Lucero, J. Y. Mutus, M. Neeley, C. Neill, P. J. O'Malley, P. Roushan, A. Shabani, V. N. Smelyanskiy, A. Vainsencher, J. Wenner, H. Neven, and J. M. Martinis, "Observation of Classical-Quantum Crossover of  $1/f$  Flux Noise and Its Paramagnetic Temperature Dependence," *Phys. Rev. Lett.*, vol. 118, p. 057702, 2017.
- [16] T. Lanting, M. H. Amin, C. Baron, M. Babcock, J. Boschee, S. Boixo, V. N. Smelyanskiy, M. Foygel, and A. G. Petukhov, "Probing Environmental Spin Polarization with Superconducting Flux Qubits," arXiv:2003.14244 [quant-ph]. [Online]. Available: <https://arxiv.org/abs/2003.14244>
- [17] "We used the python package lmfit," [https://lmfit.github.io/lmfit-py/examples/example\\_fit\\_multi\\_datasets.html](https://lmfit.github.io/lmfit-py/examples/example_fit_multi_datasets.html), accessed: 2020-06-24.